INTERNATIONAL ATOMIC ENERGY AGENCY
UNITED NATIONS EDUCATIONAL, SCIENTIFIC AND CULTURAL ORGANIZATION
INTERNATIONAL CENTRE FOR THEORETICAL PHYSICS
I.C.T.P., P.O. BOX 586, 34100 TRIESTE, ITALY, CABLE: CENTRATOM TRIESTE

UNITED NATIONS INDUSTRIAL DEVELOPMENT ORGANIZATION

INTERNATIONAL CENTRE FOR SCIENCE AND HIGH TECHNOLOGY

SMR: 630/3

MINIWORKSHOP ON NONLINEARITY: Dynamics of Surfaces in Nonlinear Physics

(13 - 24 July 1992)

"Coherent Structures in Turbulent Convection, an Experimental Study"

presented by:

A. Libchaber
NEC Research Institute
4 Independence Way
Princeton, NJ 08540
U.S.A..

Physica A 166 (1990) 387–407
North-Holland

COHERENT STRUCTURES IN TURBULENT CONVECTION, AN EXPERIMENTAL STUDY

Giovanni ZOCCHI, Elisha MOSES and Albert LIBCHABER

Department of Physics, The James Franck and Enrico Fermi Institutes, The University of Chicago, 5640 S. Ellis Avenue, Chicago, IL 60637, USA

Received 28 March 1990

We present results from a visualization experiment in Rayleigh–Bénard convection in water at high Rayleigh number. We distinguish three kinds of coherent structures in the flow: waves along the boundary layers, plumes, and spiraling swirls. The waves originate from the interaction of plumes with the boundary layers. The spiraling swirls appear to be the result of a shear instability of the viscous boundary layer. We describe the "life cycle" of these structures in the cell, and then we focus on the waves and characterize them quantitatively using local temperature measurements.

1. Introduction

Bénard convection is an interesting and convenient system for investigating turbulence experimentally. The reasons, which are clearly exposed in the introduction of a paper by Malkus [1], are mainly that the geometry is simple and the experimental parameters can be carefully controlled. In the considerable amount of work, both theoretical and experimental, which has been accumulated on the subject, attention has been focussed on the behaviour of "extensive" quantities, like the heat flux, and "intensive" ones, like the average temperature or rms temperature and velocity fluctuations, as a function of the Rayleigh and Prandtl numbers and the distance from the boundaries. In this study we take a different point of view, and try to describe the flow starting from its elementary constituents, the coherent structures.

Let us first briefly review previous work on turbulent convection. A basis for fruitful theoretical developments was provided by a theory advanced by Malkus [2]. He starts from the assumption that there is a smallest scale of motion which is effective for the heat transport. In practice, this is embodied in writing the heat flux as a Fourier series in the vertical coordinate, which is truncated at some mode. He then obtains an upper bound for the Nusselt number (the dimensionless heat flux) in the form of a scaling law: $Nu \sim Ra^{1/3}$,

and is able to calculate the rms fluctuating velocity profile. A different approach was offered by the scaling theory of Kraichnan [3]. In his work, the size of the thermal and viscous boundary layers is determined by transitional Péclet and Reynolds numbers, and from this the scaling for the heat flux and the fluctuating velocity and temperature is found, for small and large Prandtl numbers. Howard [4] gave a treatment which was more strongly motivated by the experimental evidence, in particular Townsend's observations of the relevance of thermals (buoyant blobs breaking off from the boundary layers) [5]. He proposed that the size of the thermal boundary layer could be determined by requiring that it be marginally stable against convection (which amounts to assigning a transitional Rayleigh number to the boundary layer), and could thus obtain the "classical" scaling, $Nu \sim Ra^{1/3}$, in a simple and elegant way. Howard's paper also contains a clear discussion of the theoretical work on the subject prior to 1966.

On the experimental side, accurate measurements of the profile of the average temperature and rms temperature fluctuations were performed by Townsend [5] in an "open top" convection cell in air, and found consistent with the Malkus theory. Since then, many experiments have been conducted in the same spirit, using different geometries, fluids of different Prandtl numbers, and sometimes extending the measurements to the statistical properties of the velocity field [6–13]. Concerning the scaling for the Nusselt number, most experiments find exponents slightly smaller than 1/3 [17].

Several researchers have commented on the role of thermals in turbulent convection, but without studying it in detail. As this is one type of coherent structure with which we are concerned here, let us review their observations. Townsend [5] distinguished "quiescent periods" from "periods of activity" in his temperature signals, and attributed the latter to "the detachment of columns of hot air from the edge of the conduction layer". In their interferometric study of a water convection cell, Chu and Goldstein [9] saw thermals being released from the boundary layer. For "moderate" Rayleigh numbers ($\sim 10^5$) these blobs traverse the cell vertically and cause a temperature gradient reversal just outside the opposite boundary layer, while at higher Rayleigh numbers ($\sim 10^7$) they traverse horizontally. In particular, fig. 10 of this paper shows a travelling "bulge" in the thermal boundary layer, a phenomenon which we seek to describe in detail in the present work. Tanaka and Miyata [11], examining their temperature fluctuation profiles, also came to the conclusion that for $Ra > 10^6$ the thermals released from the boundary layers do not reach the opposite plate. They also observed "buoyant plumes in the form of sheets" emitted from the boundary layers. The horizontal drift of thermal plumes was also observed by Krishnamurti and Howard [14] in a large aspect ratio cell in water, and associated with the onset of large scale flow (that

is, a coherent flow on a scale comparable to the lateral size of the box) for $Ra > 10^6$. Indeed, as already mentioned, thermals were an important physical motivation for Howard's model of a marginally stable boundary layer; in this author's words: "it is interesting to try to build a theory of convection centered on the idea of the thermals". An experimental test of Howard's ideas was recently provided by Foster and Waller [15], who, measuring the frequency of the temperature signal spectrum associated with the largest fluctuations, could determine the characteristic period τ of warm bursts, and found $\tau \sim Ra^{-1/2}$ as predicted.

In the present work, we investigate experimentally turbulent convection from the point of view of the coherent structures produced by the flow. By "coherent structure" we mean here any structure which has a lifetime comparable to its own transit time through the cell. The patterns created by these objects in the cell can be quite complex (fig. 1), yet the resulting statistical behaviour is rather simple, being governed by scaling laws throughout an impressively wide range of Rayleigh numbers [17]. It is thus conceivable that this simplicity might be captured through a "statistical mechanics" kind of treatment of the coherent structures in the flow. This study is intended as a step towards posing the problem in these terms. Fig. 1 is a shadowgraph of our convection cell in the state described below. The intricate pattern visible in the

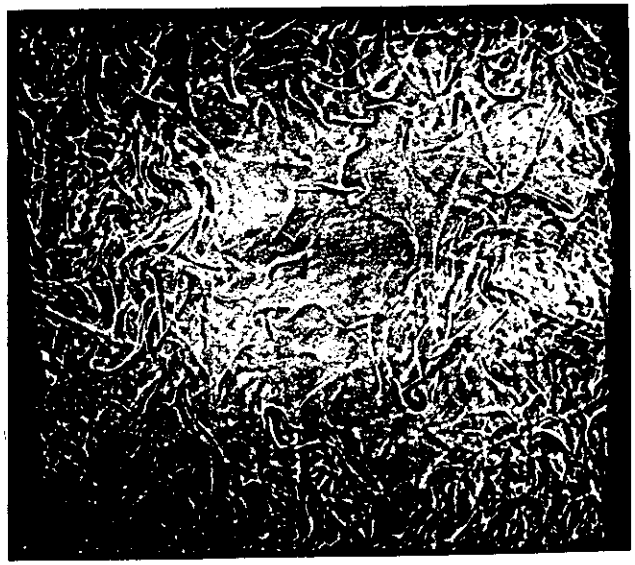

Fig. 1. Shadowgraph of the whole cell. $Ra = 1.2 \times 10^7$.

picture is formed by thermal plumes emitted from the top and bottom boundary layers. In the following, we try to categorize the coherent structures which appear in turbulent convection, completing previously reported work [16a, b]. We then focus on one kind of structure, waves in the boundary layers, and report quantitative measurements of their properties. In particular, we wanted to answer the question of whether the waves are normal modes of the boundary layer.

Our experimental system is the same as in ref. [16a]: a cubic cell filled with water, of size $L = 18.5$ cm, with brass top and bottom plates and glass walls for visualizing purposes. The bottom plate is heated at constant rate and the temperature of the top plate is regulated within 0.05°C. While taking the measurements described in section 3 the cell was insulated from the outside with styrofoam.

For a given geometry of the cell, the state of the system is completely described by two numbers, the Rayleigh number and the Prandtl number

$$\mathrm{Ra} = \frac{\alpha g \Delta L^3}{\nu\kappa}, \qquad \mathrm{Pr} = \frac{\nu}{\kappa}$$

(here α is the coefficient of thermal expansion, g the gravity acceleration, Δ the temperature difference between the bottom and top of the cell, κ the thermal diffusivity and ν the kinematic viscosity). All the measurements reported below were taken in the state $\mathrm{Ra} = 1.2 \times 10^9$, $\mathrm{Pr} = 5.6$, far above the onset of convection (which is at $\mathrm{Ra} \sim 2 \times 10^3$, independent of Pr), and in fact in a turbulent state. In section 2 we also briefly discuss some qualitative results obtained for the state $\mathrm{Ra} = 2.4 \times 10^8$, $\mathrm{Pr} = 6.1$.

The choice of state was dictated by the following considerations: it has been shown in ref. [17] that in turbulent convection there exists a scaling regime ("hard turbulence") which, at least for aspect ratios close to one, extends from $\mathrm{Ra} \sim 4 \times 10^7$ to $\mathrm{Ra} \sim 10^{12}$. The statistical properties of all these states (probability distributions of fluctuations, power spectra, etc.) are identical up to scaling. From the point of view of the flow pattern, what distinguishes this regime from the lower Rayleigh numbers, "soft turbulence" states, is perhaps the presence of a large number of thermal plumes [16a], as in fig. 1. With our choice we just pick one representative out of this class of similar states. This particular Rayleigh number was chosen because it corresponds to the temperature range of the liquid crystals we used for the visualization.

At these high Rayleigh numbers the average temperature profile (average in time) inside the cell has the following structure: the whole temperature drop occurs across two thin layers near the bottom and top plates (the thermal boundary layers), while the bulk of the fluid is isothermal. Intuitively this is because the turbulent motion in the bulk results in a "short circuit" for heat transport, so that the average temperature gradient there is very small, whereas near the plates, where the velocity goes to zero, the heat transport is predominantly diffusive, with a large temperature gradient. The size of the thermal boundary layer controls the heat transport across the cell. The classical scaling for the dimensionless heat flux Nu ($\mathrm{Nu} \sim \mathrm{Ra}^{1/3}$) is obtained by assuming that the thermal boundary layer is marginally stable to convection [2, 4]. Fig. 2 shows the measured average temperature profile near the top plate for our state ($\mathrm{Ra} = 1.2 \times 10^9$). We have called T_0 the temperature of the plate, and h is the distance from the plate. The temperature drop across this boundary layer is 3.90°C = $\Delta/2$, half of the total temperature drop across the cell.

Let us get an idea of the Rayleigh and Reynolds numbers relevant for the boundary layers. From the construction indicated by the solid lines in fig. 2 we obtain the size of the thermal boundary layer $\delta_T = 1.1$ mm. We can then calculate the corresponding Rayleigh number of the boundary layer,

$$\mathrm{Ra}^{\mathrm{b.l.}} = \frac{\alpha g (\Delta/2) \delta_T^3}{\nu\kappa} \approx 130 .$$

This is one order of magnitude smaller than the value of ~ 2800 extracted by Howard [4] from Townsend's data in air. This discrepancy has its origin, we believe, in the different large scale flows present in the two experiments, due to the different boundary conditions. The data of Tanaka and Miyata [11] for $\mathrm{Ra} = 2 \times 10^9$ in a cell of aspect ratio about 3 ($\delta = 1.4$ mm, $L = 20$ cm) give $\mathrm{Ra}^{\mathrm{b.l.}} = 700$, while Castaing et al. [17] measure $\mathrm{Ra}^{\mathrm{b.l.}} = 130$ in an aspect ratio 1 cell in He gas at $\mathrm{Ra} = 10^9$. We will see later (fig. 5c) that the average large scale

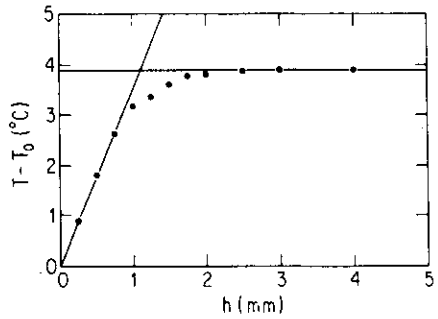

Fig. 2. Average temperature profile near the top of the cell; T_0 is the temperature of the upper plate, and h is the distance from the plate.

velocity in the region near the plates is of the order of $u \sim 5$ mm/s, so that the Reynolds number of the thermal boundary layer is $\mathrm{Re} = u\delta/\nu \approx 5$. Also from fig. 7b we infer a size of the viscous boundary layer δ_v of the order of 5 mm, which, with a typical velocity of ~ 5 mm/s, gives a corresponding Reynolds number of about 25. This ratio of sizes of the viscous to the thermal boundary layer is consistent with Kraichnan's estimate [3], $\delta_v/\delta_t \sim (10 \times \mathrm{Pr})^{1/2}$, which, for our Prandtl number, gives $\delta_v/\delta_t \sim 7$.

2. The visualization

In the state which we are describing ($\mathrm{Ra} = 1.2 \times 10^9$) there is a stable large scale flow in the cell, with fluid flowing up along one corner, diagonally across the plate and down along the opposite corner. Similar flows have been observed at high Ra, both for large and small aspect ratio cells [14, 6]. Our observations were performed using commercial liquid crystals encapsulated in microspheres (50–100 μm sphere diameter) suspended in very low concentrations ($\sim 10^{-4}$ by weight) in the flow. One obtains thus a qualitative picture of the temperature field (through the color change of the liquid crystals), and also of the velocity field (by following the motion of the particles) [18]. To investigate two different convection states, we used two different liquid crystal samples: the first one would turn from red to green to blue in a temperature window of about 4°C around 29°C, and was used for the higher Rayleigh number state. The second one had a window of 1°C around 25°C, thus allowing us to visualize for a Rayleigh number four times smaller. It turns out that this factor of four is enough to observe at least the trend of what seems to be the different characteristics of the flow in soft and hard turbulence. We obtained the best contrast by illuminating a small region of the cell with a beam of white light and observing the light scattered at $\sim 90°$. For observing the waves in the boundary layer we used a thin sheet of light shone grazing to the boundary layer surface.

By these means, we came to the following qualitative conclusions concerning the flow in the higher Rayleigh number state: warm plumes rise mainly along one corner and the neighboring sides of the cell, cold plumes fall along the opposite corner and sides. Let us follow a typical warm plume: it is formed from the lower boundary layer and is carried by the flow close to a corner. While it rises, the cap grows in size and has reached a few cm in diameter by the time it is close to the top plate. When it collides with the upper boundary layer it starts a front, which is visible as a circular perturbation traveling along the thermal boundary layer, much like the circular waves produced by a stone tossed into a pond. In Plate Ia–c we show the development of such a

disturbance; the field of view is the entire bottom plate, and we use a sheet of light about 3 mm thick. Similar waves have been observed by Elder [6] travelling up and down the vertical plates of a convection slot (of aspect ratio $\sim 1/20$) with a horizontal temperature gradient.

The effect of a plume splashing into the boundary layer is thus to create a "kink" in it, and to set it in motion because of the flow which the plume creates, which is similar to a jet directed into the plate. In fact a plume seems paricularly suited to excite such a traveling kink because of the structure of the velocity field in the cap, which resembles a dipole [19], or a Rankine flow [20]. We believe that it is the velocity field created by the plume which is important in this process, not its temperature field. In fact, we have artificially shot small, hot plumes from a heater against the upper plate; their effect is then merely to annihilate the thermal boundary layer where they hit, without starting an appreciable kink. In contrast to this, we were able to excite these perturbations by directing a jet of "cold" water from a nozzle onto the upper boundary layer.

The question is now whether the perturbation created by the plume excites a propagating mode of the viscous boundary layer, or whether the wave which we observe is still the same plume which expands horizontally when it hits the plate, much like a vortex ring would do. In the first case the picture is one of coherent structures (the plumes) exciting normal modes of the viscous boundary layer, while in the second one we have just plumes (or thermals; see later) interacting with a plate. In either case, this gives rise to a disturbance which travels along the viscous boundary layer, which is, in our case, thicker than the thermal boundary layer. The velocity field of this disturbance would then drive the waves which we observe in the thermal boundary layer, the temperature behaving rather as a "passive scalar", a dye with which the fluid is marked, so to speak, with no important dynamic effects.

After an initial acceleration imparted by the plume's velocity field, the newly formed kink continues to travel at approximately constant speed unless the large scale flow changes, or unless it collides with another wave. In our higher Rayleigh number state ($\mathrm{Ra} = 1.2 \times 10^9$) the large scale flow is rather stable, and most of the rising and falling plumes are bunched together along opposite corners of the cell, so that most waves are formed in one corner of the top or bottom plate (see later fig. 5a) and travel across that plate with little interactions with other waves. Under these circumstances we observe the development of what we believe is a shear instability on top of the waves, which produces, locally along the wavefront, spiraling structures like the ones shown in Plate IIa,b. This picture is obtained by illuminating a small region of the cell near the upper plate. We see in cross section the plate, the cold fluid of the upper boundary layer (red) and the warmer fluid of the bulk (green). The spiral (which is traveling from right to left with the large scale flow) is formed

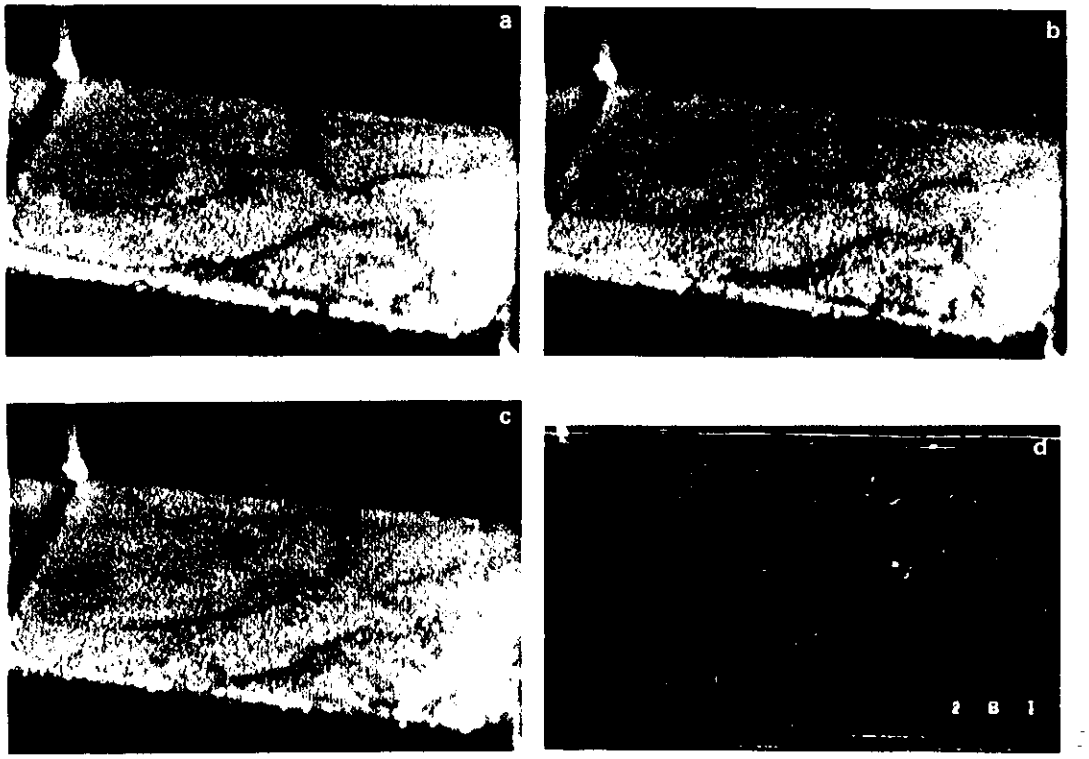

Plate I. (a, b, c) Waves in the lower boundary layer expanding outwards from the point where the corresponding plumes hit the bottom. The time interval between the pictures is of the order of a second. Cold fluid is red, hotter fluid is green and the waves are visible as darker lines. (d) This is a different visualization of the bottom boundary layer (the details are explained in the text) showing waves (the curved, broader structures) and secondary instabilities (plumes and swirls) which ride on the wavefronts.

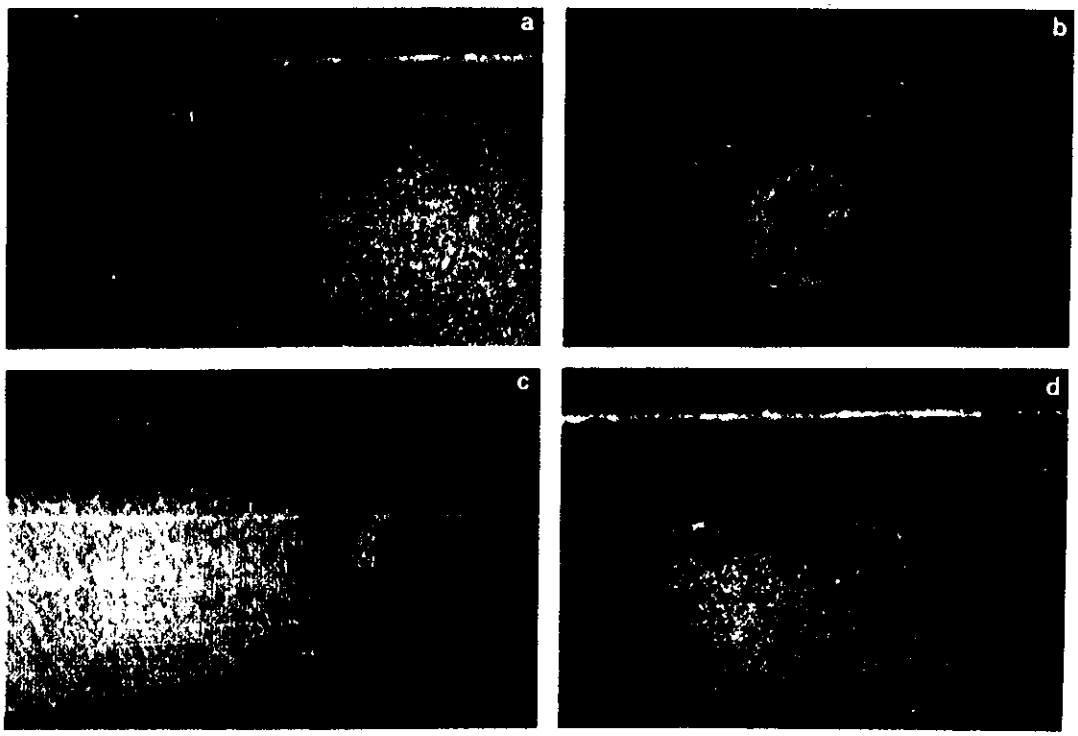

Plate II. (a, b) Spiraling swirls gliding along the upper boundary layer (the motion is from right to left). The cold fluid of the boundary layer is red, the warmer fluid of the bulk green and blue. The field of view is about 2 cm. (c, d) Thermal plumes emitted from the upper boundary layer. Note the waves in (d), which appear as smaller protuberances of the boundary layer.

by cold fluid from the boundary layer. In contrast to plumes, which for many purposes can be adequately repesented by a simple potential flow [20], vorticity is probably an essential ingredient for describing these structures. Their shape is very reminiscent of the spirals in the Kelvin–Helmholtz instability [21]. We have not yet explored in detail the lateral structure of these objects. They are certainly localized, and seem to contain vorticity, but then, since a vortex line must close either on itself or on a boundary, there is a question of whether this structure can be roughly described as a vortex tube in the form of a hook attached to the plate.

As it keeps moving across the plate, our typical wave eventually gets to a region, near the opposite corner of the cell, where the horizontal large scale velocity drops to zero. Here buoyancy dominates over inertia, and cold fluid just falls, forming plumes. There are already "open channels" for the boundary layer to leak down, namely the spiraling swirls formed previously, and new channels, i.e. starting plumes, are formed, this process being now reminiscent of the Rayleigh–Taylor instability [21] in a stratified fluid. Plate IIc,d shows such starting plumes. These cold plumes, traveling down along the corner of the cell, will hit the bottom boundary layer and excite new waves, which in turn will propagate towards the opposite end of the cell and give rise to hot plumes, thereby closing the "life cycle" of the cell.

It is worth mentioning that in our description so far we have not distinguished between "plumes", which consist of a column of buoyant fluid emanating from the boundary layer and culminating in a cap, and "thermals", which are buoyant blobs not connected to the boundary layer. Although a plume will become a thermal if its stem is cut off, the dynamics of the two structures is very different: while a plume can be described by a potential flow [20], a thermal is more similar to a buoyant vortex ring [22]. In suggestive words, a plume is a non-dissipative bound state, while a thermal is a dissipative free particle state. In the cell, a buoyant instability always starts as a plume (Plate IIc,d). However, as it grows taller the stem is likely to undergo an instability caused by the surrounding fluctuating flow, and to release the cap, which becomes a thermal. In fact a stem can in this way release successively several thermals. Thus the objects which reach the opposite boundary layer and produce the waves are probably mostly thermals.

In summary, from direct visual observations we obtain the following qualitative picture: there are two kinds of "excitations": those which live in the bulk of the cell, the plumes and the spiraling swirls, and the others, the waves, which live along the boundary layers. Plumes hitting the boundary layers excite waves; these are sustained by the coherent large scale flow, and they further decay to spiraling swirls, if inertia dominates over buoyancy, or plumes in the opposite case (there are actually intermediate cases also). The plumes thus

formed, when they hit the opposite boundary layer, in turn excite new waves, and so on. Fig. 3 is a schematic drawing depicting this process.

We are now in a position to correctly interpret a picture like Plate Id, which is similar to the ones published in ref. [16a]. The technique here is to shine a thin sheet of light (with no liquid crystals in the fluid now) at almost grazing incidence to the boundary layer and observe the light scattered by the bottom plate at $\sim 90°$. The incoming beam consists of alternate bright and dark stripes (interference fringes), and deformations of the temperature profile in the boundary layer can be observed as deformations of this pattern of stripes. This visualization can be somewhat misleading, because structures in the cell, which actually extend vertically from the bottom, will appear, because of the projection, as straight lines across the plate. Thus the strikingly straight lines in Plate Id are actually projections of the "base" of swirls or plumes extending upwards. But we nonetheless can see in the picture waves (the broader, somewhat curved fronts) and swirls or plumes shooting up at localized spots along the wave fronts.

In the same cell, we have looked at a lower Rayleigh number state ($Ra = 2.4 \times 10^8$). We can summarize the observations by saying that, in contrast to the previous state, here buoyancy appears to dominate over inertia throughout the cell. That is, cold fluid always falls and warm fluid rises. Accordingly, there are no spiraling swirls but only plumes. Furthermore, in this case the "waves" are perhaps more appropriately described as domain boun-

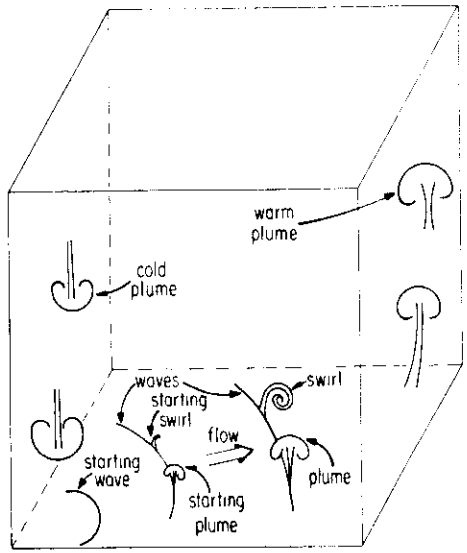

Fig. 3. The "life cycle" of the cell.

daries, in the following sense: hot plumes (say) no longer rise mainly along one corner, but go up through a broader region of the cell. Thus it is common, for example, for two plumes to hit simultaneously adjacent corners of the top plate. The respective outgoing flows will run into each other somewhere halfway across the plate, defining a line, which can be almost stationary, along which fluid flows down in a sheet. This is a boundary between two domains, with fluid rising at the center of the domains and falling at the border between them. Thus the characteristic feature of this state is not excitations sustained by a coherent large scale flow, but a slower dynamics of "domain boundaries". While there is a clear difference betwen the two regimes, because of our limited range in Rayleigh number we can only report a trend, rather than a clear cut transition. In the next section we turn to a more quantitative characterization of the waves in the higher Rayleigh number state ($Ra = 1.2 \times 10^9$).

3. The measurements

The task of extracting, from recordings of the temperature fluctuations at different points (fig. 4), the signal of the waves and measuring their properties, is in some respects similar to the one of isolating and characterizing the relevant events in a high energy physics experiment. Our "particles", the waves, have a characteristic signature, which has to be separated from the "noise" caused by other events, which in our case are other fluctuations. Some care must be taken with the detection system; for example, we did not get reliable results until we realized that the detectors should not be placed directly behind each other with respect to the waves' direction. Otherwise the wake of the first detector will cause a noticeable distortion in the shape of the wave seen at the second detector. Another important detail was the position of the probes along the plate; they had to be placed not too far from the corner where most waves originated so as to catch many waves, yet far enough downstream so that the waves would have attained their asymptotic form. Like in a particle physics experiment, we were not sure in the beginning whether we would obtain reliable statistics. Eventually everything came to a happy ending, but it took much loving care, whispered threats, and understanding, among our equipment and ourselves.

In what follows we describe our measuring and analysis procedures in detail, then proceed to present the results of these measurements. In summary, the results are that we establish the waves as independent objects with well defined characteristics. We measure their velocity and wavelength, and find that a correlation exists, which can be interpreted in terms of a simple dispersion

relation for interface waves. We then probe the internal structure of their temperaure and velocity field, and find it consistent with propagation of a coupled velocity–temperature wave. In particular, we show that the amplitude of the thermal excitations is significant within the thermal boundary layer, although their origin probably lies in a perturbation propagating along the viscous boundary layer.

The Chicago wave detector (CWD) consists of four temperature probes (commerical semiconductor thermistors) mounted in horizontal pairs. The distance between probes within each pair was $D = 3.10$ mm. One pair could be moved up and down close to the top plate by means of a micrometer, while the other pair was fixed at a distance of 1.50 mm from the plate, near the "surface" of the upper boundary layer (see fig. 2). Each probe yielded the time series of the temperature at that point: the four resistances were measured using four ac driven bridges; the outputs were amplified and digitized simultaneously with a typical sampling rate of 20 Hz per channel, and stored for analysis. Fig. 4 shows portions of such time series taken with the probes all at the same height; the two upper signals are from the moveable probes, the two lower ones from the other pair. The scale shown on the ordinate, $\Delta/2$, is the temperature drop across the boundary layer; the temperature is plotted reversed, that is up is cold and down is warm. We have stacked the four signals on top of each other for ease of comparison.

We can see from fig. 4 that when a wave hits the detector it is seen as a "cold" spike in the signal. Since the boundary layer near the top plate is colder than the fluid in the bulk, this indicates that the waves are essentially a bulge

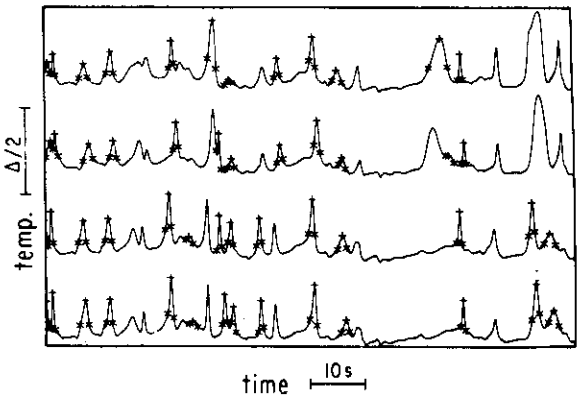

Fig. 4. Portion of a typical time series (100 s) recorded by the four probes. The crosses and stars mark the points chosen by the "pattern recognition program" to calculate velocity, amplitude, etc. of the waves.

protruding out of the boundary layer, a local vertical enhancement of the boundary layer size. Our analysis is based on identifying such spikes and measuring their amplitude and width. The relevant points for this are marked on fig. 4, crosses showing the maxima and stars indicating the points where the amplitude (measured from a baseline defined by averaging) has dropped by a factor $1/e$. We can now compute the time of flight of a wave between the two probes of each pair and obtain the velocity. However, the "pattern recognition program" makes many mistakes: it is evident from fig. 4 that some waves are missed, and sometimes a secondary spike is identified instead of the principal one, which will result in wrong values of the velocity, wavelength and amplitude for that wave. The problem is that, from the point of view of extracting the waves, we have to deal with a rather "noisy" signal, as is apparent from fig. 4. The reader is reminded that we are measuring the characteristics of these structures in a turbulent flow, so that we encounter the same kind of difficulties one would have in trying to determine the properties of sea waves by watching a system of buoys bob up and down in a storm. To reduce the number of mistakes, we used a "trigger" based on coincidences, that is an event is taken as a wave if the corresponding signals on the two pairs of probes are within a certain time window of each other. We have checked the accidental coincidence rate to be small. The wave assignments shown in fig. 4 are before enforcement of the trigger condition.

The details of the algorithm are as follows: first, we found that the fastest way of pinpointing a wave candidate was to scan the difference signal of the two probes for places where it cuts through zero with a large enough slope. This indicates that on the two signals there are two spikes close enough to be correlated, and yet far enough so that they do not completely overlap (i.e. the transit time is well defined). Then we demand that the slope at the zero crossing be, say, positive. This ensures that we measure only waves coming from one side of the cell (we would of course choose the sign of the slope that corresponds to the direction from which most of the waves come). Finally we look at the individual probe time records, seaching for a spike either to the left or right of the zero crossing point of the difference signal, depending on which probe in the pair is expected to be hit first by the wave. A spike must be found on each channel for the event to count as a wave. At various stages of the analysis a "Monte Carlo simulation" of the waves was useful in checking the efficiency of the wave-finder algorithm.

Having ascertained that a wave has been registered by both probes, we can compute its velocity as the distance between the probes divided by the transit time. Clearly the problem now is that the angle of incidence of the wave enters in both the velocity and the wavelength, and cannot be obtained using only two probes. To eliminate this angle dependence we used the data from the second

pair of probes. We could produce two different types of measurements, in the following way. One – we call them *absolute* measurements – were obtained with the moveable probes at the same height as the fixed ones. The four probes would then be arranged at the corners of a rectangle contained in a plane parallel to the plate, the length of the sides of this rectangle being $D = 3.10$ mm and $S = 4.60$ mm (the distance between the two pairs of probes). With this geometry we could measure in two orthogonal directions, thereby obtaining the amplitude and direction of the velocity, and the wavelength (that is, the width in the direction of motion) of the waves. The graphs of fig. 5 are constructed with these measurements. Also, in this way we could obtain two independent measurements for each wave (by pairing the four detectors differently), check the results for consistency, and use the average of the two measurements.

A second method for eliminating the angular dependence, while obtaining information on the vertical structure of the waves, was to take what we call *relative* measurements. For this we would position the moveable probes at different heights and would take the ratio of the velocities, amplitudes, etc., measured by these probes and the fixed ones. Since the two pairs had the same orientation, we were measuring the same projection, and the angular term was divided out with this procedure. We could thus probe within one wave the structure of the translational velocity, the amplitude and wavelength as a function of height. The graphs of fig. 7 are constructed in this way.

Let us now examine the absolute measurements of the velocity, wavelength, etc., which were obtained, as mentioned before, with both pairs of probes at the same distance $h = 1.50$ mm from the plate. All the graphs in fig. 5 are constructed using the same set of about 5000 waves, taken over a period of 17 hours. Fig. 5a is a histogram of the direction of the waves' velocity (the quantity on the abscissa is the angle between the velocity of the wave and the side of the box). Most prominent is the peak at $\sim 45°$, which corresponds to waves coming from the corner of the plate. This is what we expect, with hot plumes climbing along the corner of the cell, splashing against the upper boundary layer and thus emitting the wave. There is however another, smaller peak at $\sim 0°$, which indicates that a significant amount of waves come from the center of one of the adjacent sides of the plate. The pictures in Plate I are consistent with this result; they show several waves, one emanating from the center of the left side, and the others having started near the left rear corner of the bottom plate.

Fig. 5b shows the histogram of the amplitude of the waves. While the amplitude is limited by $\Delta/2$, we see that the distribution is rather broad, indicating that the velocity field associated with the perturbation can shuffle cold fluid from different depths of the boundary layer.

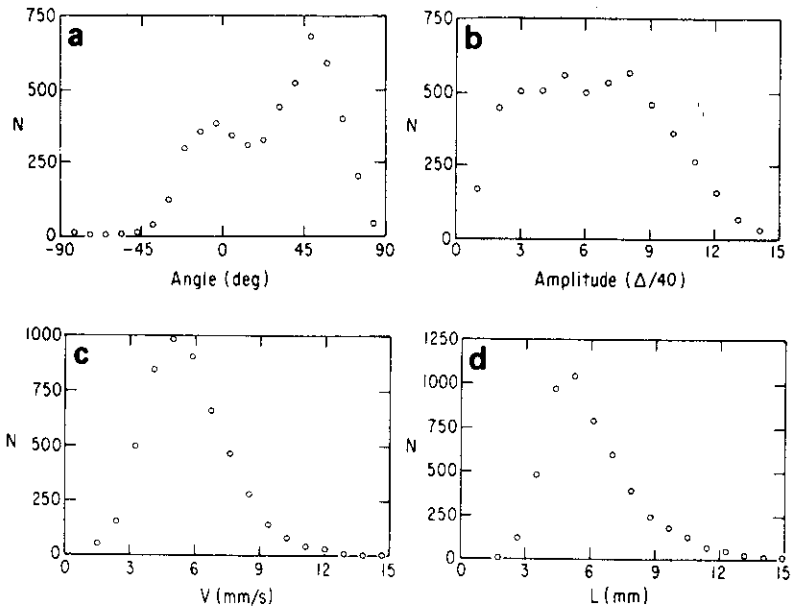

Fig. 5. (a) Histogram of the direction of the velocity of the waves. The angle is counted with respect to one side of the plate. The peak at ~ 45° is due to waves coming from the corner of the plate, the other peak corresponds to waves coming from the center of one adjacent side. (b) Histogram of the amplitude of the waves. The scale on the abscissa is in units of $(\Delta/2)/20$, where $\Delta/2$ is the temperature drop across the boundary layer. N is the number of counts. (c) Histogram of the magnitude of the velocity of the waves. (d) Histogram of the wavelength of the waves.

Fig. 5c is the histogram of the velocity. The distribution is rather narrowly peaked around 5.7 mm/s, with a standard deviation of 2.0 mm/s, and seems to correspond to the velocity of the large scale flow in the cell. In fig. 5d we report the corresponding graph for the width, or "wavelength", of the waves. It is very similar to the velocity distribution, both in the shape of the peak and its width. It centers around 6.2 mm, with a standard deviation of 2.2 mm. While the narrowness of the peak in the velocity distribution may be linked to the characteristics of the large scale flow in the cell, for the width of the waves this is probably not so. In fact, we interpret the latter measurement as an indication that the waves are independent excitations of the boundary layers.

From the similarity of the width distribution to that of the velocity we infer that these two quantities may be correlated for the waves. Indeed, one might want to ask whether there is a simple dispersion relation which holds for these waves. Fig. 6a is a plot of the magnitude of the velocity v vs. the "wavelength" (width) L. Each dot corresponds to the measured values for a single wave, and

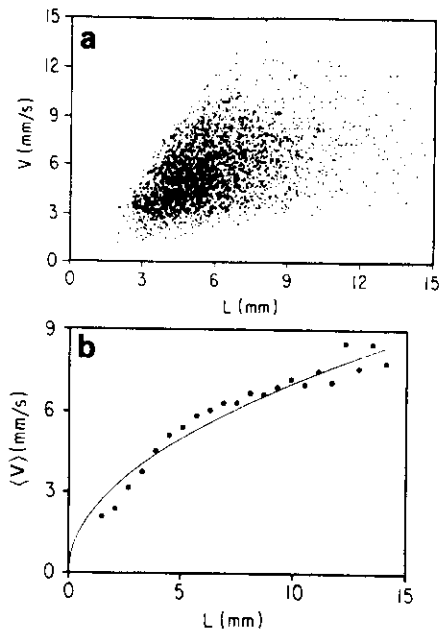

Fig. 6. (a) Plot of the velocity vs. wavelength using a sample of ~ 3000 waves out of the ~ 5000 waves in this run. (b) This graph is obtained from (a) by binning the wavelength and averaging over the values of the velocity for the full sample of ~ 5000 waves. Dots are at the center of the bin, and represent the data. The solid line is a fit to a gravity-wave-like dispersion relation.

the graph is constructed with about 3000 waves. We see that there is no simple functional relationship between velocity and wavelength, but rather the experimental points are contained within an angular sector in the v–L plane. On average, though, the velocity increases with wavelength, in the sense that if one computes, from fig. 6a, for each value of L the average of the corresponding values of v, one finds an increasing function of L. In contrast to this, the plots of amplitude vs. velocity or amplitude vs. wavelength do not show any correlation between these quantities.

At this point, it is perhaps not superfluous to reassure the reader that the spread of the points in fig. 6a is not just due to mistakes in the wave assignments: as mentioned before, with four probes we can construct two independent measurements of a wave and we have checked that selecting the waves according to a stringent requirement on the consistency of these two measurements does not alter the result.

If we perform the above-mentioned averaging on the points of fig. 6a, we obtain the graph shown in fig. 6b. We see that this average velocity $\langle V \rangle$

increases approximately as the square root of the wavelength L. The solid line in the graph is a fit of the data to the form $\langle V \rangle = \frac{1}{2}(aL/2\pi)^{1/2}$, which comes from the dispersion relation for gravity waves: $\omega^2 = ak$ (k is the wave vector). The spirit of this analysis is that the waves are normal modes of the boundary layer, and that they are similar to gravity driven waves at the interface between two fluids of different densities, which here are the colder fluid of the top boundary layer and the warmer fluid of the bulk. But our waves are also affected by the fluctuating "wind" due to the turbulent large scale flow in the cell, which could be the origin of the spread in velocities of fig. 6a. Averaging over this fluctuating wind would then restore the "true" dispersion relation (fig. 6b). The obvious difficulty is that our stratification is unstable, in other words, the parameter a here should be negative. Nevertheless, we note that the numerical value we obtain from the fit, $a = 12.5\ \mathrm{cm/s^2}$, is reasonable compared to what we would expect in terms of this simple two fluids model, which is $a = (\rho_1 - \rho_2)/(\rho_1 + \rho_2)g$ where ρ_1 and ρ_2 are the densities of the heavier and lighter fluid, respectively, and g is the acceleration of gravity. For our temperature jump $\Delta/2 = 3.90°\mathrm{C}$ across the boundary layer this would give $a = 0.6\ \mathrm{cm/s^2}$. Of course, at this level this is really only a dimensional analysis argument; in particular, as already noted, the sign of a is wrong.

While the above discussion is appealing, we must keep in mind that the origin of this speculation lies in the measurements displayed in fig. 6a. Our justification of the averaging procedure which leads to fig. 6b is plausible, but no more than that.

We now turn to the relative measurements, with which we can probe the internal structure of the waves. In the graphs of fig. 7, each point represents an average over about 1000 waves. We note that the statistical deviation on such samples is small, as is reflected by the smoothness of the data. In fig. 7a we plot the relative amplitude A_r of the temperature disturbance associated with the wave as a function of the distance from the plate, h. The reference height is that of the fixed probes, $h = 1.5$ mm, and there $A_r = 1$, as we expect (the graph has not been normalized to impose this condition). The point closest to the plate, $h = 0.25$ mm, was taken with the moveable probes touching the plate; because the probes themselves have a diameter of 0.5 mm, this measurement was plotted at $h = 0.25$ mm. This figure shows that, as far as the temperature is concerned, these excitations live at the surface of the thermal boundary layer: the amplitude is maximum for $h = 1$ mm, which corresponds to the size δ_T of the boundary layer (fig. 2). This is reminiscent of interface waves (e.g. gravity waves on Lake Michigan), where the amplitude drops exponentially with the distance from the interface. However, the amplitude in fig. 7a does not drop to zero for large h, but rather tapers off to a constant value. Since we have no visual evidence for such an elongated protrusion of the wave, we believe the

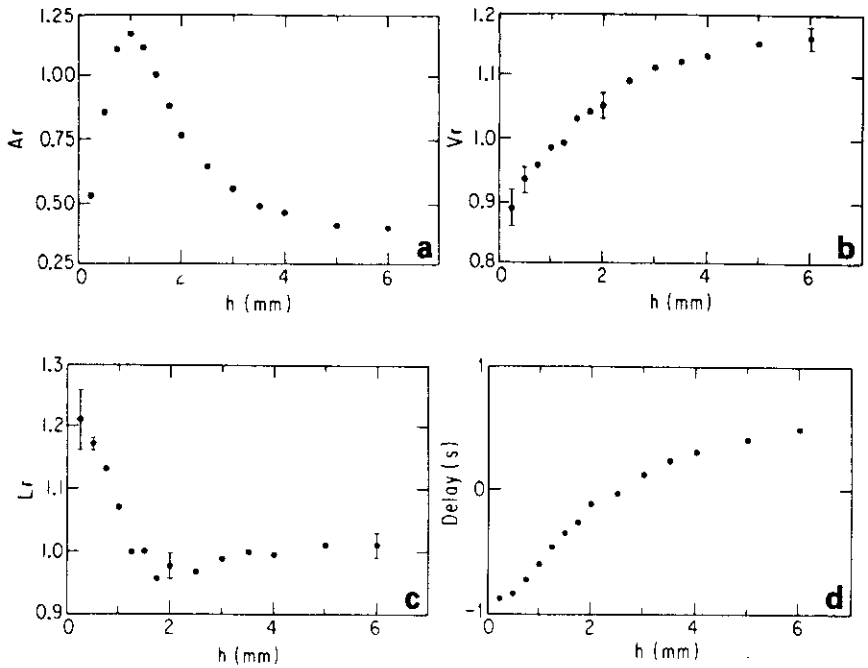

Fig. 7. Relative measurements as a function of height h. (a) Relative amplitude (= Ampl.(h)/Ampl.(h_0), where $h_0 = 1.5$ mm). (b) Relative velocity (the error bars show statistical errors). (c) Relative wavelength (width in the direction of motion). (d) Delay between the passage of the waves at the first and at the second pair of probes. This graph, rotated by 90° and with the time axis appropriately rescaled, shows the average shape in space of the structures.

tail at large h in the graph to be due to the contribution of the "stems" of forming plumes and swirls, which ride on localized regions of the waves and extend vertically. If this is indeed the case than this asymptotic value of A_r would give the probability of a plume or swirl to be found on the wave.

Fig. 7b shows the relative velocity V_r. If the "waves" were simply blobs of hotter or colder fluid flowing along the plate, we would expect $V_r \to 0$ for $h \to 0$, that is, the graph should just show the velocity profile of a viscous boundary layer. As this is not the case, the velocity field of these objects must have a more complex structure. For interface waves, we would of course expect $V_r = \mathrm{const.} = 1$. The fact that V_r is not constant here means that the waves undergo a considerable amount of stretching during their lifetime.

The at first sight surprising result that a temperature perturbation can propagate in a wavelike fashion along the thermal boundary layer is of course due to the fact that the temperature field is coupled to the velocity field

through an advection term. Thus a wave of the velocity field in the shear layer near the plate would give rise to a traveling temperature perturbation.

From the relative wavelength measurements, fig. 7c, we do not gain much new information. The width of the perturbation is essentially constant with height, with a slightly broader "foot" inside the thermal boundary layer. Here and in fig. 7b the error bars show statistical errors. Finally, in fig. 7d we plot the delay between the arrival of the wave at the first and at the second pair of detectors. As one expects from the relative velocity measurements (fig. 7b) this shows that the structure is on average tilted in the direction of motion. Since typical velocities and wavelengths are of the order of ~ 5 mm/s and ~ 5 mm, respectively (see fig. 5), and since the distance between the two pairs of probes is $S = 4.60$ mm, we see that the tilt corresponding to a 1 s delay is of the order of one wavelength.

In summary, the main purpose of this section is to show that it was in this case possible to isolate from a complicated looking time series like the one in fig. 4 the signature of one type of excitation, the waves, and probe their internal structure in some detail while they move in the turbulent flow. The main issue is now whether the waves are normal modes of the boundary layer. The measurements displayed in fig. 6 support this conjecture, while the failure to excite these waves by, for example, shaking the boundary layer locally, leaves the question open.

4. Epilogue

In the first part of this paper we have seen how the complicated looking flow of fig. 1 is organized. It is a small world of its own, with clouds and rain, wind and storms. We have described the "life cycle" of the cell qualitatively, and we would now like to set about understanding it quantitatively. Accordingly, we take a first step in this direction by focusing on the waves and measuring their properties. There are other coherent structures in the flow, and it will be necessary to understand the dynamics of each one separately, and then proceed to study the behaviour of a collection of them. Part of this program has already been attacked [20], and more work is planned for the future.

The measurements described in the present report suffer from one obvious limitation: although we recognize the importance of the viscous boundary layer in propagating excitations across the cell, we do not directly probe its velocity field, because we only measure temperatures. The observation of what looks like shear instabilities that carries away parts of the thermal boundary layer (Plate IIa,b), raises important questions; for example, the Howard–Malkus marginal stability argument for the thermal boundary layer [2, 4] may have to

be modified if it is to be applied to this regime. This work thus leads us to direct our attention towards the viscous boundary layer and its instabilities.

We would like to thank Professor J. Gollub for bringing the liquid crystals visualization technique to our attention, and Dr. M. Parsley, of Hallcrest Inc., for kindly supplying us with the samples with which the experiment was conducted. We benefitted from discussions with Professor M. Shelley, who is developing a stability analysis for the viscous boundary layer. One of us would like to take this opportunity to recall the happy, thoughtless year spent roaming through the charms of Chicago with Steve Gross, who actually built the experimental cell and initiated the observations. G.Z. presents this work as a thesis to the Department of Physics, The University of Chicago, in partial fulfillment of the requirements for the Ph.D. degree. This work was supported by NSF grants DMR 8722714 and MRL 8819860. E.M. acknowledges the support of a Weizmann Postdoctoral Fellowship.

References

[1] W.V.R. Malkus, Proc. R. Soc. London A 225 (1954) 185.
[2] W.V.R. Malkus, Proc. R. Soc. London A 225 (1954) 196.
[3] R.H. Kraichnan, Phys. Fluids 5 (1962) 1374.
[4] L.N. Howard, Proc. 11th Int. Congress of Appl. Mech., H. Gortler, ed. (Springer, Berlin, 1966) p. 1109.
[5] A.A. Townsend, J. Fluid Mech. 5 (1959) 209.
[6] J.W. Elder, J. Fluid Mech. 23 (1965) 99.
[7] J.W. Deardorff and G.E. Willis, J. Fluid Mech. 28 (1967) 675.
[8] A.M. Garon and R.J. Goldstein, Phys. Fluids 16 (1973) 1818.
[9] T.Y. Chu and R.J. Goldstein, J. Fluid Mech. 60 (1973) 141.
[10] D.E. Fitzjarrald, J. Fluid Mech. 73 (1976) 693.
[11] H. Tanaka and H. Miyata, Int. J. Heat Mass Transfer 23 (1980) 1273.
[12] R.J. Goldstein and S. Tokuda, Int. J. Heat Mass Transfer 23 (1980) 738.
[13] D.C. Threlfall, J. Fluid Mech. 67 (1975) 17.
[14] R. Krishnamurti and L.N. Howard, Proc. Natl. Acad. Sci. 78 (1981) 4.
[15] T.J. Foster and S. Waller, Phys. Fluids 28 (1985) 455.
[16a] S. Gross, G. Zocchi and A. Libchaber, Compt. Rend. Acad. Sci. (Paris) 307 (1988) 447.
[16b] G. Zocchi, S. Gross and A. Libchaber, in: Random Fluctuations and Pattern Growth: Experiments and Methods, NATO ASI Series, E. Stanley and N. Ostrowsky, eds. (Kluwer, London, 1988) p. 275.
[17] B. Castaing, G. Gunaratne, F. Heslot, L. Kadanoff, A. Libchaber, S. Thomae, X. Wu, S. Zaleski and G. Zanetti, J. Fluid Mech. 204 (1989) 1.
[18] T.H. Solomon and J.P. Gollub, Sheared boundary layers in turbulent Rayleigh–Bénard convection, preprint 1990.
[19] D.J. Shlien and R.L. Boxman, Int. J. Heat Mass Trans. 24 (1981) 919.
[20] E. Moses, G. Zocchi, I. Procaccia and A. Libchaber, The dynamics and interactions of laminar thermal plumes, preprint (1990).
[21] S. Chandrasekhar, Hydrodynamic and Hydromagnetic Stability (Dover, New York, 1981).
[22] J.S. Turner, Proc. R. Soc. London A 239 (1957) 61.